

RAMAN STUDIES ON CARBON-CONTAINING PHASES IN  
NANOSIZED-ZrO<sub>2</sub>/C AND NANOSIZED-(ZrC,ZrO<sub>2</sub>)/C COMPOSITES

A. Martiz<sup>1,2</sup>, A. Farkas<sup>3</sup>, Z. Karoly<sup>1</sup>, F. P. Franguelli<sup>1,4</sup>,  
S. K. Samaniego<sup>1</sup>, A. Menyhard<sup>1</sup>, L. Kotai<sup>2,5</sup>

<sup>1</sup> Budapest University of Technology and Economics  
Department of Physical Chemistry and Materials Science  
Budapest, Hungary

[josalmar20@gmail.com](mailto:josalmar20@gmail.com)

<sup>2</sup> Research Centre for Natural Sciences  
Institute of Materials and Environmental Chemistry  
Budapest, Hungary  
[kotai.laszlo@ttk.hu](mailto:kotai.laszlo@ttk.hu)

<sup>3</sup> Budapest University of Technology and Economics  
Department of Organic Chemistry and Technology  
Budapest, Hungary

<sup>4</sup> Budapest University of Technology and Economics  
Department of Inorganic and Analytical Chemistry  
Budapest, Hungary

<sup>5</sup> Deuton-X Ltd.  
Erd, Hungary

Accepted 2022 January 17

**Abstract**

Raman spectroscopic studies were performed to identify the nature of the carbon-containing phases in nano-(ZrC,ZrO<sub>2</sub>)/C composites. The nano-ZrO<sub>2</sub>/C composites were prepared in a tube furnace by heat-treatment of zirconium-loaded sulfonated styrene-divinylbenzene resins between 1000 and 1400 °C. The plasma processing of a nano-ZrO<sub>2</sub>/C sample in inert or reducing atmosphere resulted in nano-(ZrC,ZrO<sub>2</sub>)/C composites. The Raman spectra of the nano-ZrO<sub>2</sub>/C samples show that the ratio of the amorphous carbon / graphitic components decreases, whereas the fraction of distorted graphite structures increases with increasing reaction temperature and time. This can be attributed to the formation of new graphene edges by the condensation of the polyene content in the amorphous carbon. The ratio of the amorphous carbon practically does not change if the plasma treatment was performed under inert (Ar+He) atmosphere. In contrast, under reducing (Ar+H<sub>2</sub>) atmosphere, the amorphous carbon almost completely crystallizes into graphite. The ratio of the defective / regular graphite structures and the change of the thickness or separation of the graphene (monolayer carbon) sheets are higher under inert than reducing plasma conditions. We found no catalytic effect of ZrC on the graphite crystallization under inert plasma conditions, but in the presence of H<sub>2</sub>, ZrC may catalyze the graphitization process.

## 1. Introduction

Zirconium carbide–carbon (ZrC/C) composites belong to the important strategic materials in emitters and coatings developed for nuclear reactor fuels due to their extremely high melting point, mechanical strength, small neutron absorption cross-section, high sorption capacity, and (radiolytic) stability towards radioactive isotopes [1 – 4].

The main routes to synthesize ZrC/C composites are solid-state reactions of elementary carbon and Zr or Zr-compounds like ZrH<sub>2</sub> or ZrO<sub>2</sub> [5, 6], or the reactions of zirconium or its compounds like Zr-acetate or oxychloride with organic carbon sources such as methyl halides [7 – 10]. In another method, Zr-loaded polymers, especially ion exchangers are carbonized under various conditions including plasma-assisted heat treatments [3, 4, 11 – 13]. It results (ZrC,ZrO<sub>2</sub>)/C composites with adjustable ZrC content and various forms of carbon phases. The zirconium carbide in such composites generally contains some carbon vacancies [6]. However, the reaction of carbon-deficient ZrC<sub>x</sub> structures with the free carbon-content of the ZrC/C composites results in the formation of non-stoichiometric Zr<sub>1-x</sub>C (carbon-rich) materials which increase their sinterability [14].

In this paper we studied the nano-(ZrC,ZrO<sub>2</sub>)/C composites and their nano-ZrO<sub>2</sub>/C precursors prepared from sulfonated styrene-divinylbenzene copolymers [11] by Raman spectroscopy to reveal the properties of the carbon phases in the composites.

The samples prepared in a tube-furnace were labeled as X-DVB-Zr-T-t, where X, T and t stand for the DVB content in the initial sample, the pyrolysis temperature (1000, 1200 and 1400 °C) and the reaction time (2 or 8 h), respectively.

In addition, 8-DVB-Zr-1000-2 sample was subjected to plasma processing under inert (Ar+He) or reducing (Ar+H<sub>2</sub>) conditions. The samples were labeled as 8-DVB-Zr-He and 8-DVB-Zr-H<sub>2</sub>, respectively.

## 2. Experimental

### 2.1. Preparation of samples

Varion KS samples and zirconyl chloride were supplied by Deuton-X Ltd (Erd, Hungary). Preparation of zirconium-loaded sulfonated Varion KS-2 and KS-8 resin is described in [11] using zirconyl chloride octahydrate (0.5 mass % Zr, in 3 M HCl). These resin samples were ground in a planetary ball mill (225 rpm, 30 min), and pyrolyzed in an alumina tubular furnace under Ar atmosphere at 1000, 1200 and 1400 °C for 2 or 8 h in each case. The ZrO<sub>2</sub>@C sample prepared by pyrolysis at 1000 °C for 2 h was subjected to a further in-flight thermal plasma treatment in an inert (He) or a reducing (H<sub>2</sub>) atmosphere. Detailed descriptions of the plasma processing are available in [11, 15, 16].

A Horiba Jobin–Yvon LabRAM-type micro-spectrometer was used with an external laser source of 532 nm Nd-YAG for Raman spectroscopy. The laser beam was focused on an objective of 20X (numerical aperture = 0.4). A confocal hole of 1000 μm was used in the confocal system, and a grating monochromator of 1800 mm<sup>-1</sup> was used for light dispersion. The detected wavenumber was scanned with 3 cm<sup>-1</sup> of resolution, 60 s of accumulation time per point, in a spectral range of 200 – 3400 cm<sup>-1</sup>.

### 3. Results and discussions

#### 3.1. Preparation and properties of Zr-loaded ion-exchangers (2-DVB-Zr and 8-DVB-Zr)

Two styrene-divinylbenzene copolymer-based sulfonated ion-exchangers with 2 and 8 wt. % divinylbenzene content and 1.69 and 1.63 average sulphonation degree/ring were loaded with zirconyl chloride ( $\text{ZrOCl}_2 \cdot 8\text{H}_2\text{O}$ ) in a 3 M HCl solution as detailed in [11]. The maximum Zr-loading was not higher than ca. 80 % because mainly the p-position sulfonic acid groups are capable of fixing zirconium, whereas the sterically unfavorable o-position sulfonic acid groups cannot bind the zirconyl ions [11].

#### 3.2. Thermal decomposition of Zr-loaded Varion KS ion-exchangers

The styrene-DVB copolymers decompose on heating with the formation of solid carbonaceous materials and liquid / gaseous hydrocarbons [17, 18]. The proportion of the solid / liquid / gaseous decomposition products and the hardness of the solid residue strongly depend on the DVB content, sulfonation degree and the metal content of the modified resin [18 – 20]. Metal loading of the sulfonated ion exchangers results in a higher production yield of the solid fraction. Additionally, the sulfonate groups are converted into  $\text{SO}_2$  or metal sulfides, if the metals are sulfidophilic [19, 21]. Due to Zr–O bonds in the starting Zr-loaded ion-exchangers, stable nanosized  $\text{ZrO}_2$  polymorphs (tetragonal, monoclinic and cubic) containing carbon composites were formed [11]. XRD analysis revealed the formation of graphitic and amorphous carbon, too, the amount of which depends on the reaction conditions [11] (Table 1). RF thermal plasma treatment of the 8-DVB-ZrO<sub>2</sub>-1000-2 sample was performed under inert (Ar + He) and reducing atmospheres (Ar+H<sub>2</sub>).

**Table 1.** Carbon composition of nano-ZrO<sub>2</sub>/C and nano-(ZrO<sub>2</sub>,ZrC)/C composites from XRD.

Sample	Carbon content (XRD), wt. %		Graphite / amorphous carbon ratio
	Graphite	Amorphous carbon	
2-DVB-Zr-1000-2	~ 50	~ 15	~ 3.3
2-DVB-Zr-1200-2	~ 45	~ 30	~ 1.5
2-DVB-Zr-1400-2	~ 40	~ 45	~ 0.9
2-DVB-Zr-1400-8	~ 20	~ 60	~ 0.3
8-DVB-Zr-1000-2	~ 30	~ 60	~ 0.5
8-DVB-Zr-1200-2	~ 25	~ 65	~ 0.3
8-DVB-Zr-1400-2	~ 30	~ 65	< 0.5
8-DVB-Zr-1400-8	~ 20	~ 75	< 0.4
8-DVB-Zr-He	~ 55	–	–
8-DVB-Zr-H <sub>2</sub>	~ 55	–	–

With increasing temperature during pyrolysis, the graphite content showed decreasing tendency for the 2 % DVB containing samples. In contrast, little changes without any definite trend could be found in the case of samples with 8 % DVB content. The decreased graphite content is unexpected because the higher temperature and prolonged time should promote crystallization and graphitization.

These results most probably can be attributed to the inaccuracy of the XRD method for comparing the proportion of crystalline and amorphous carbonaceous phases. Therefore, to characterize the amorphous / graphitic carbon phases in these samples, we performed detailed Raman studies with deconvolution of the Raman band structures.

### 3.3. Raman studies on nano-ZrO<sub>2</sub>/C and nano-(ZrO<sub>2</sub>,ZrC)/C samples

Due to the amorphous carbon content and defects in graphite, powder XRD analysis is not suitable for the reliable characterization of the carbon matrix in the prepared nano-ZrO<sub>2</sub>/C and nano-(ZrO<sub>2</sub>,ZrC)/C samples. In contrast, Raman spectroscopy is sensitive not only to changes in the crystalline but also in the molecular structures (long-range order). Hence, the Raman spectra of graphite or graphite-like materials resulting from lattice vibrations are sensitive to the presence and degree of structural disorders. This allows determining the degree of graphitization by Raman spectroscopy [22 – 27].

Highly ordered monocrystalline graphite has two first-order Raman bands (G) and G1 (2D) at around 1580 and 2687 cm<sup>-1</sup> (E<sub>2g</sub> symmetry, degenerated optical mode at the center of Brillouin zone, and harmonic in-plane transverse optical mode close to the zone boundary K point, respectively [28 – 30], ideal graphite lattice).

The disordered graphitic lattice has a band D1 (D) around and D2 (D') at around 1350 and 1620 cm<sup>-1</sup>, respectively (A<sub>1g</sub> and E<sub>2g</sub> symmetry, phonon of the in-plane longitudinal optical branch close to the zone center, and the in-plane acoustic branch close to the K point, or graphene layer edges and surfaces, respectively) [31 – 34].

D3 (D'' or A) band characterizes the amorphous carbon at ca. 1500 cm<sup>-1</sup>, whereas D4 (I) band at ca. 1200 cm<sup>-1</sup> contains the disordered graphite lattice (A<sub>1g</sub>) or polyenes and ionic impurities induced modes [22, 25, 35, 36]. The second-order Raman spectra of carbonaceous materials contain weak D+D'' combination and 2D' harmonic overtone bands [37 – 39].

The Raman spectra of nano-ZrO<sub>2</sub>/C samples made from 2 % DVB containing Zr-loaded Varion KS by heat treatment at 1000 (a) and 1200 °C (b) for 2 h and at 1400 °C for 2 h (c) and 8 h (d), respectively, are illustrated in Figure 1.

The positions and assignment of the Raman shifts after deconvolution are summarized in Table 2. Both the peak intensity of D'' bands (amorphous carbon) and the intensity ratio of D''/(D+D'+G) peaks (amorphous / all graphitic component) gradually decrease with increasing the reaction temperature and time, which suggests advancing graphitization.

The intensity ratio of D/G bands slightly increases with increasing heating temperature, while the increase is more pronounced with prolonged time indicating the increased fraction of the distorted graphite. The D4 peak intensities decrease, whereas the D1 peak intensities increase (new graphene edges) with increasing the reaction time and temperature, which can be attributed to the formation of new graphene edges by condensation of polyenes in the amorphous carbon.

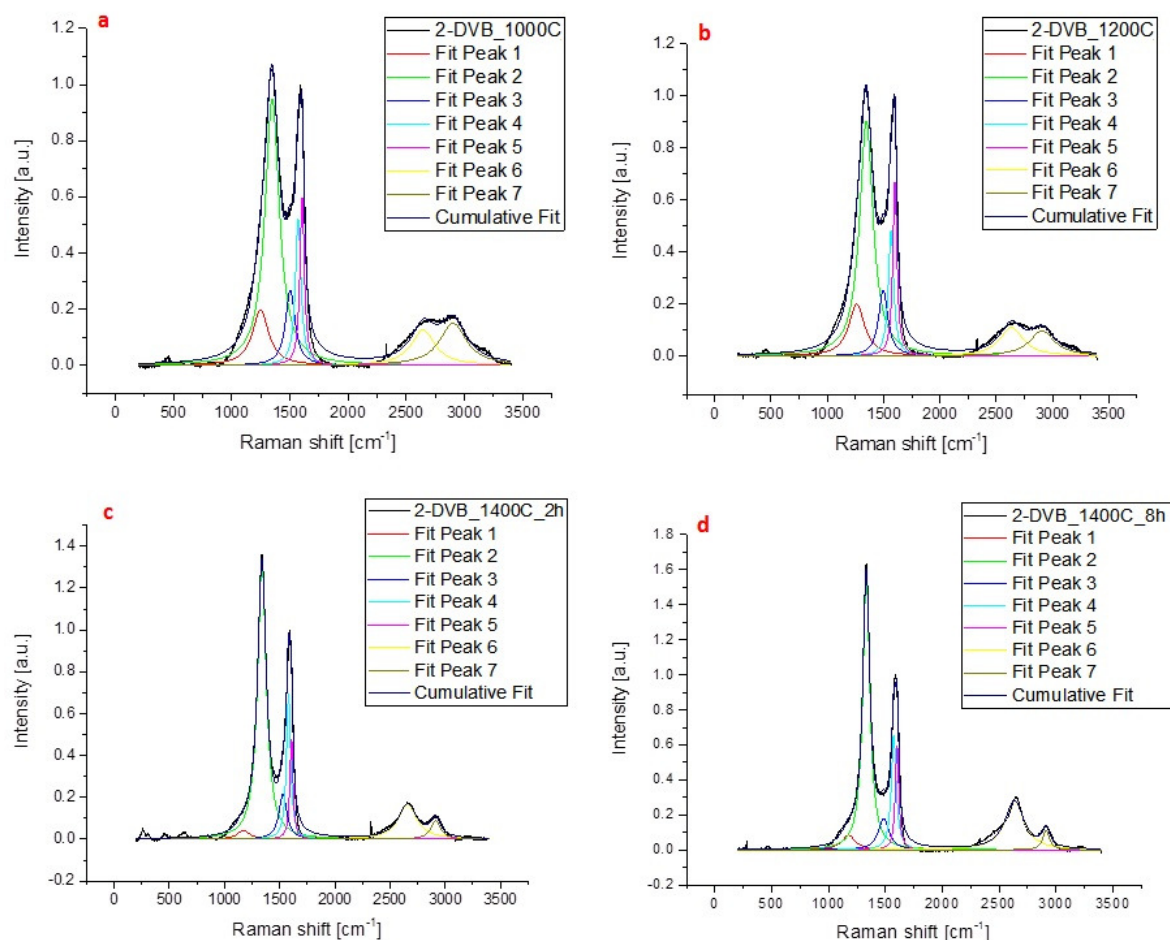


**Figure 1.** Raman spectra of nano-ZrO<sub>2</sub>/C samples made from 2 % DVB containing Zr-loaded Varion KS by heat treatment at 1000 (a) and 1200 °C (b) for 2 h and at 1400 °C for 2 (c) and 8 h (d), respectively.

**Table 2.** Raman bands of nano-ZrO<sub>2</sub>/C samples made from 2 % DVB containing Zr-loaded Varion KS by heat treatment at 1000 and 1200 °C for 2 h and at 1400 °C for 2 and 8 h.

Sample	Raman shifts in cm <sup>-1</sup> / intensities							Raman shift intensity ratios		
	D* (D4)	D (D1)	D'' (D3)	G	D' (D2)	2D (G1)	D+D'	I <sub>D</sub> /I <sub>G</sub>	I <sub>D</sub> '/I <sub>G</sub>	I <sub>D</sub> '/I <sub>D+D'+G</sub>
2-DVB-Zr-1000-2	1247 (0.20)	1347 (0.95)	1503 (0.27)	1571 (0.52)	1605 (0.60)	2645 (0.13)	2902 (0.15)	1.81	0.24	0.13
2-DVB-Zr-1200-2	1260 (0.20)	1346 (0.90)	1496 (0.25)	1565 (0.48)	1600 (0.67)	2634 (0.11)	2906 (0.10)	1.88	0.23	0.12
2-DVB-Zr-1400-2	1171 (0.04)	1339 (1.32)	1530 (0.22)	1580 (0.69)	1606 (0.48)	2658 (0.16)	2913 (0.09)	1.91	0.24	0.09
2-DVB-Zr-1400-8	1175 (0.08)	1331 (1.56)	1484 (0.18)	1573 (0.66)	1602 (0.60)	2635 (0.28)	2913 (0.11)	2.38	0.43	0.06

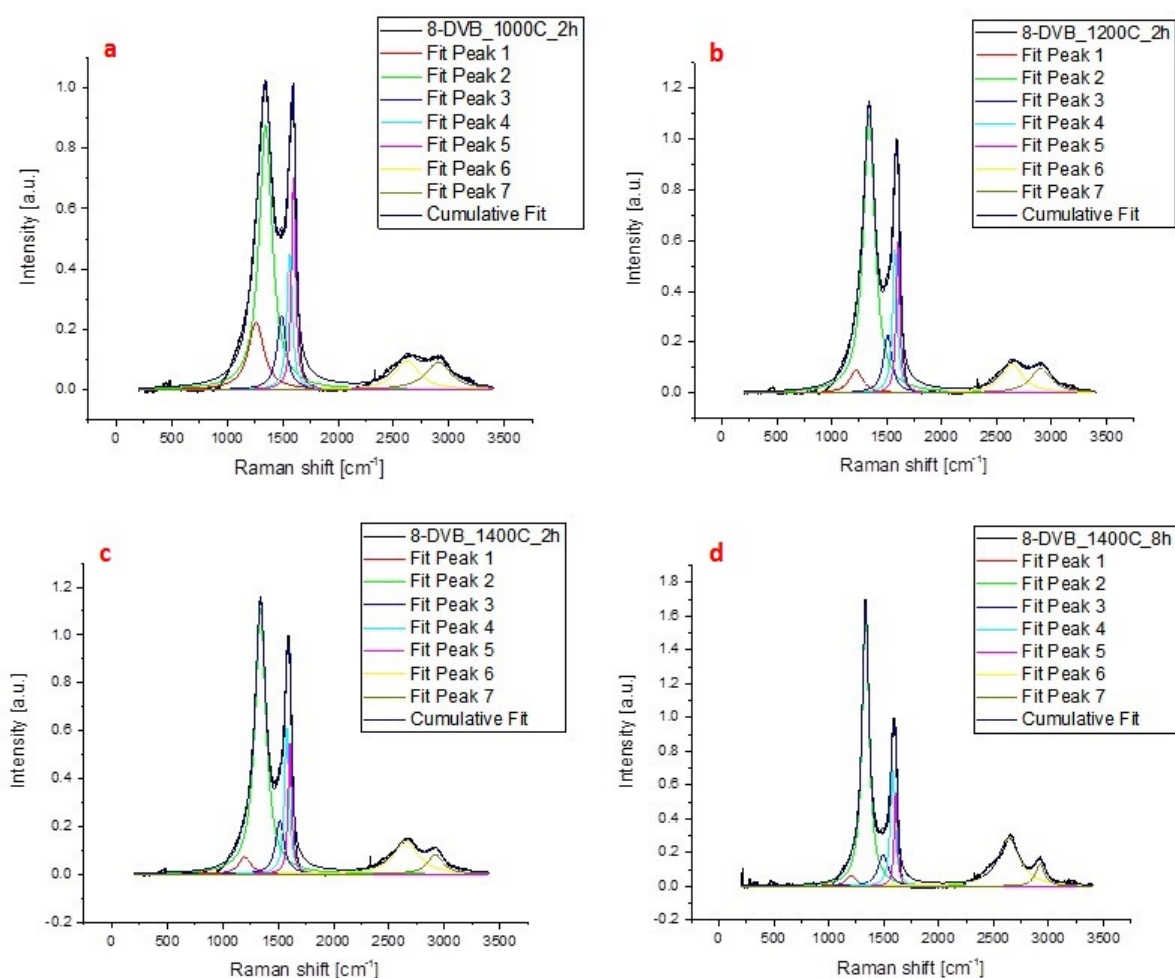


**Figure 2.** Raman spectra of nano-ZrO<sub>2</sub>/C samples made from 8 % DVB containing Zr-loaded Varion KS by heat treatment at 1000 (a) and 1200 °C (b) for 2 h and at 1400 °C for 2 (c) and 8 h (d), respectively.

**Table 3.** Raman bands of nano-ZrO<sub>2</sub>/C samples made from 8 % DVB containing Zr-loaded Varion KS by heat treatment at 1000 and 1200 °C for 2 h and at 1400 °C for 2 and 8 h.

Sample	Raman shifts in cm <sup>-1</sup> / intensities							Raman shift intensity ratios		
	D* (D4)	D (D1)	D'' (D3)	G	D' (D2)	2D (G1)	D+D'	I <sub>D</sub> /I <sub>G</sub>	I <sub>D</sub> /I <sub>G</sub>	I <sub>D'</sub> /I <sub>D+D'+G</sub>
8-DVB-Zr-1000-2	1260 (0.22)	1347 (0.88)	1491 (0.25)	1563 (0.45)	1599 (0.70)	2623 (0.10)	2903 (0.09)	1.94	0.21	0.12
8-DVB-Zr-1200-2	1220 (0.09)	1339 (1.09)	1509 (0.23)	1574 (0.57)	1603 (0.60)	2642 (0.11)	2902 (0.10)	1.93	0.20	0.10
8-DVB-Zr-1400-2	1200 (0.07)	1341 (1.11)	1516 (0.22)	1578 (0.61)	1606 (0.55)	2652 (0.14)	2917 (0.08)	1.81	0.23	0.09
8-DVB-Zr-1400-8	1204 (0.06)	1335 (1.63)	1495 (0.19)	1581 (0.69)	1609 (0.55)	2638 (0.28)	2922 (0.13)	2.37	0.41	0.07

The Raman spectra of nano-ZrO<sub>2</sub>/C samples made from 8 % DVB containing Zr-loaded Varion KS by heat treatment at 1000 (a) and 1200 °C (b) for 2 h and at 1400 °C for 2 (c) and 8 h (d), respectively, are shown in **Figure 2**. Peak positions and their assignment are summarized in **Table 3**. The general tendencies are practically similar to the samples made from 2 % DVB containing Zr-loaded ion exchangers. The intensity ratio of D''/(D+D'+G) (amorphous /all graphitic component) gradually decreases with increasing the reaction temperature and time according to the progress of graphitization. On the other hand, the intensity ratio of D/G bands is hardly affected by the heating temperature, however increases with prolonged reaction time. Similar to 2 % DVB containing samples, the D4 peak intensities decrease here, too. The D1 peak also rises with increasing reaction time and temperature, which shows the formation of new graphene edges. These above results show that the powder XRD analysis is inadequate to determine the ratio of amorphous carbon / graphite components in the nano-ZrO<sub>2</sub>/C composites. Raman spectroscopy, however, is suitable to follow even the quantitative changes among the different carbonaceous materials like amorphous carbon, graphite and distorted graphite structures.

Furthermore, the 2D Raman band intensity reflects the ABAB stacking and the crystal sizes [39]. The  $I_{2D}/I_G$  ratio relates to the thickness or separation of the graphene (monolayer carbon) sheets. This parameter changed for both type of resin samples only when they were subjected for a longer period (8 h) of heat treatment at 1400 °C. The increase in the amount of distorted graphite structures may be attributed to the Zr intercalation effect onto the carbons structures [40]. In contrast, the catalytic effect of ZrC on the graphitization process [40] can be neglected because no ZrC formation could be detected from the ZrO<sub>2</sub> and amorphous carbon / graphite reactions [11] below 1400 °C. The formation of ZrC was detected only above 1500 °C in the ZrO<sub>2</sub>/C systems [40].

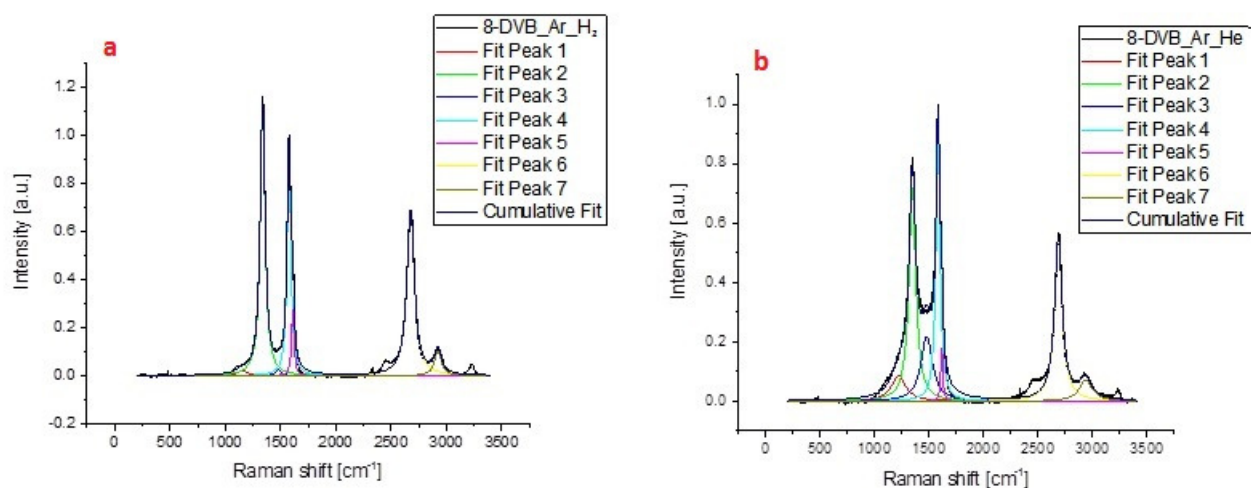


**Figure 3.** Raman spectra of nano-ZrO<sub>2</sub>/C samples made from 8 % DVB containing Zr-loaded Varion KS by RF-plasma treatment under H<sub>2</sub> (a) and He (b) atmospheres.

In order to study the possible catalytic effect of the ZrC content on the graphitization process, RF thermal plasma tests have been carried out in inert (Ar+He) and reducing (Ar+H<sub>2</sub>) atmospheres. The relative amounts of the amorphous and graphitic carbon structures and their state was investigated by Raman spectroscopy, too (see **Figure 3** and **Table 4**).

**Table 4.** Raman bands of nano-ZrO<sub>2</sub>/C samples made from 8 % DVB containing Zr-loaded Varion KS at 1000 °C, and by RF-plasma treatment under H<sub>2</sub> and He atmospheres.

Sample	Raman shifts in cm <sup>-1</sup> /intensities							Raman shift intensity ratios		
	D* (D4)	D (D1)	D" (D3)	G	D' (D2)	2D (G1)	D+D'	I <sub>D</sub> /I <sub>G</sub>	I <sub>D'</sub> /I <sub>G</sub>	I <sub>D'</sub> /I <sub>D+D'+G</sub>
8-DVB- Zr-1000-2	1260 (0.22)	1347 (0.88)	1491 (0.25)	1563 (0.45)	1599 (0.70)	2623 (0.10)	2903 (0.09)	1.94	0.21	0.12
8-DVB- Zr-1200-2	1156 (0.02)	1339 (1.14)	1480 (0.03)	1577 (0.95)	1611 (0.28)	2677 (0.69)	2924 (0.10)	1.20	0.72	0.01
8-DVB- Zr-1400-2	1218 (0.08)	1345 (0.72)	1477 (0.22)	1580 (0.89)	1614 (0.18)	2685 (0.54)	2935 (0.07)	0.81	0.61	0.12

The ratio of the amorphous carbon practically did not change if the plasma treatment was performed in inert (He enriched) atmosphere. In contrast, in reducing (H<sub>2</sub> enriched) atmosphere the amorphous fraction almost completely disappeared. The ratio of distorted / regular graphite structures was also decreased on plasma treatment that can be attributed to the building up of regular graphite structures. The change in the defective / regular graphite ratio is greater under inert than reducing plasma conditions. Similar trend was found for the thickness or separation of the graphene (monolayer carbon) sheets (*I<sub>D</sub>/I<sub>G</sub>* ratio). The relative amount of surface graphene defects decreased in inert but increased in reducing atmosphere, whereas the edge-type defects decreased in both samples, but to a greater extent in inert than in reducing atmosphere. ZrC reportedly has a catalytic effect on the graphite crystallization [40], but the ZrC content in the prepared composite samples resulted in significantly different conversion ratio of the amorphous to graphite carbon content depending on the applied plasma conditions. In inert atmosphere, practically not any amorphous carbon was transformed into graphite, whereas under reducing atmosphere the transformation was almost complete. It shows that the presence of ZrC may not be the sole factor responsible for the transformation of amorphous carbon into graphite, but the presence of H<sub>2</sub> also has a significant contribution.

#### 4. Conclusion

Raman spectra of graphitic and other carbons found in the nano-ZrO<sub>2</sub>/C and nano-(ZrO<sub>2</sub>,ZrC)/C composites was studied. The nanostructured composite was prepared by the pyrolysis of modified resins under various conditions between 1000 and 1400 °C for 2 or 8 h. Some of the pyrolyzed composites were also subjected to a subsequent plasma treatment in reducing or inert atmosphere. The composite composed in part of carbonaceous material but the powder XRD analysis did not give accurate results to determine the amorphous carbon to graphite ratio in the product. Raman spectroscopy, however, proved to be a useful tool to gain information on the ratio of amorphous carbon to graphite, the fraction of the defective graphite structure and on the change of the thickness / separation of the graphene (monolayer carbon) sheets. The effect of the plasma treatment greatly depended on the applied plasma conditions.

The amorphous carbon content in the ZrO<sub>2</sub>/C sample was not changed under inert conditions but almost completely disappeared under reducing (H<sub>2</sub> containing) atmosphere. It shows that the presence of ZrC alone is not enough to catalyze the transformation of amorphous carbon into graphite. However the ZrC catalyzed graphitization can be promoted with H<sub>2</sub>. The amount of regular graphite structure is higher in the samples subjected to plasma treatment than in the samples fabricated only in the tubular furnace not higher than 1400 °C.

## Acknowledgments

The research was supported by the European Union and the State of Hungary (co-financed by the European Regional Development Fund, VEKOP-2.3.2-16-2017-00013).

## References

- [1] G. Liu, L. Cheng, K. Li, Z. Chen, X. Xiong, X. Luan. Damage behavior of atomic oxygen on zirconium carbide coating modified carbon / carbon composite. *Ceram. Int.*, 2020, 3, 3324-3331.
- [2] H. O. Pierson. *Handbook of Refractory Carbides and Nitrides: Properties, Characteristics, Processing and Applications*. 1997, Noyes Publ.
- [3] N. Scales, J. Chen, R. D. Aughterson, I. Karatchevtseva, A. Stopic, G. R. Lumpkin, V. Luca. Porous ZrC-carbon microspheres as potential insoluble target matrices for production of <sup>188</sup>W/<sup>188</sup>Re. *J. Radioanal. Nucl. Chem.*, 2018, 318, 2, 835-847.
- [4] N. Scales, J. Chen, T. L. Hanley, D. P. Riley, G. R. Lumpkin, V. Luca. Hierarchically porous carbon-zirconium carbide spheres as potentially reusable transmutation targets. *Micropor. Mesopor. Mater.*, 2015, 212, 100-109.
- [5] M. X. Zhang, Q. D. Hu, B. Huang, J. G. Li. Fabrication of ZrC particles and its formation mechanism by self-propagating high-temperature synthesis from Fe-Zr-C elemental powders. *J. Alloys Comp.*, 2011, 509, 31, 8120-8125.
- [6] T. I. Alekseeva, G. V. Galevsky, V. V. Rudneva, A. N. Cherepanov, L. Stafetsky, S. G. Galevsky. Analysis of modern production of zirconium carbide. *IoP Conf. Ser.: Mater. Sci. Eng.*, 2018, 411, 012006 (1-4).
- [7] K. Ikawa, K. Iwamoto. Coating microspheres with zirconium carbide-carbon alloy. *J. Nucl. Mater.*, 1974, 52, 1, 128-130.
- [8] K. Ikawa. Vapor deposition of zirconium carbide-carbon composites by the chloride process. *J. Less-Comm. Met.*, 1972, 29, 3, 233-239.
- [9] J. X. Wang, D. W. Ni, S. M. Dong, G. Yang, Y. F. Gao, Y. M. Kan, X. W. Chen, Y. P. Cao, X. Zhang. Synthesis of nanocrystallized zirconium carbide based on an aqueous solution-derived precursor. *RSC Adv.*, 2017, 7, 37, 22722-22727.
- [10] F. Li, X. Huang, G. J. Zhang. Scalable foaming assisted synthesis of ZrC nanopowder by carbothermal reduction. *Ceram. Int.*, 2015, 41, 3335-3338.
- [11] A. Martiz, Z. Karoly, L. Trif, M. Mohai, L. Bereczki, P. Nemeth, Zs. Molnar, A. Menyhard, R. P. Pawar, S. Tekale, L. Kotai. Plasma-assisted preparation of nano-(ZrC,ZrO<sub>2</sub>)@carbon composites from Zr-loaded sulfonated styrene-divinylbenzene copolymers. *J. Therm. Anal. Calorimetry*, 2022. – *accepted to publish*.
- [12] M. D. Sacks, C. A. Wang, Z. Yang, A. Jain. Carbothermal reduction synthesis of nanocrystalline zirconium carbide and hafnium carbide powders using solution-derived precursors. *J. Mater. Sci.*, 2004, 39, 19, 6057-6066.
- [13] A. Martiz, Z. Karoly, E. Bodis, P. Fazekas, M. Mohai, I. Bertoti, A. M. Keszler. In-flight synthesis of nanosized ZrC particles from various precursors in RF-thermal plasma. *Period. Polytech. Chem. Eng.*, 2021, 65, 3, 331-342.
- [14] Y. Zhou, T. W. Heitmann, E. Bohannan, J. C. Schaeperkoetter, W. G. Fahrenholtz, G. E. Hilmas. Carbon vacancy ordering in zirconium carbide powder. *J. Am. Ceram. Soc.*, 2020, 103, 4, 2891-2898.
- [15] P. Fazekas, E. Bodis, A. M. Keszler, Z. Czegeny, S. Klebert, Z. Karoly, J. Szepvolgyi. Decomposition of chlorobenzene by thermal plasma processing. *Plasma Chem. Plasma Proc.*, 2013, 33, 4, 765-778.

- [16] P. Fazekas, Z. Czegeny, J. Mink, E. Bodis, S. Klebert, C. Nemeth, A. M. Keszler, Z. Karoly, J. Szepvolgyi. Decomposition of poly(vinyl chloride) in inductively coupled radiofrequency thermal plasma. *Chem. Eng. J.*, 2016, 302, 163-171.
- [17] T. Kocsis, Z. May, Z. Czegeny, B. Sreedhar, R. P. Pawar, L. Kotai. Perspectives of magnetic and nanosized metal-containing amorphous carbon composite chemisorbents and catalysts. *Nano Studies*, 2016, 14, 7-35.
- [18] V. S. Komarov, M. I. Yatsevskaya, O. A. Sycheva. Properties of activated carbon produced from spent ion-exchange resins. *Dokl. Akad. Nauk BSSR*, 1985, 29, 11, 1010-1023.
- [19] L. Kotai, T. Pasinszki, Z. Czegeny, S. Balint, I. Sajo, Z. May, P. Nemeth, Z. Karoly, P. K. Sharma, V. Sharma, K. Banerji. Metal and metal-sulphide containing carbons from sulphonated styrene-divinylbenzene copolymer based ion-exchangers. *Eur. Chem. Bull.*, 2012, 1, 10, 398-400.
- [20] N. Shigeharu, H. Shinichi. Preparation of carbon products. *JPS57191213 (A)*, C01B31/02, 1981.
- [21] T. Pasinszki, M. Krebsz, D. Chand, L. Kotai, Z. Homonnay, I. E. Sajo, T. Vaczi. Carbon microspheres decorated with iron sulfide nanoparticles for mercury(II) removal from water. *J. Mater. Sci.*, 2020, 55, 4, 1425-1435.
- [22] J. B. Donnet. Black and white fillers and tire compounds. *Rubber Chem. Technol.*, 1998, 71, 323-341.
- [23] L. Bokobza. Elastomeric composites based on nanospherical particles and carbon nanotubes: A comparative study. *Rubber Chem. Technol.*, 2013, 86, 423-448.
- [24] M. Moniruzzaman, K. I. Winey. Polymer nanocomposites containing carbon nanotubes. *Macromolecules*, 2006, 39, 5194-5205.
- [25] V. Singh, D. Joung, L. Zhai, S. Das, S. I. Khondaker, S. Seal. Graphene-based materials: Past, present and future. *Prog. Mater. Sci.*, 2011, 56, 1178-1271.
- [26] H. Kim, C. W. Macosko. Processing-property relationships of polycarbonate / graphene composites. *Polymer*, 2009, 50, 3797-3809.
- [27] M. Hernandez, M. del Mar Bernal, R. Verdejo, T. A. Ezquerro, M. A. Lopez-Manchado, Overall performance of natural rubber / graphene nanocomposites. *Compos. Sci. Technol.*, 2012, 73, 40-46.
- [28] J. F. Rabolt, R. Santo, J. D. Swalen. Raman measurements on thin polymer-films and organic monolayers. *Appl. Spectrosc.*, 1980, 34, 517-521.
- [29] F. Adar, M. Delhaye, E. Da Silva. Evolution of instrumentation for detection of the Raman effect as driven by available technologies and by developing applications. *J. Chem. Edu.*, 2007, 84, 50-60.
- [30] D. A. Long. Early history of the Raman effect. *Int. Rev. Phys. Chem.*, 1988, 7, 317-349.
- [31] M. Maiti, M. Bhattacharya, A. K. Bhowmick. Elastomer nanocomposites. *Rubber Chem. Technol.*, 2008, 81, 384-469.
- [32] J. R. Potts, D. R. Dreyer, C. W. Bielawski, R. S. Ruoff. Graphene-based polymer nanocomposites. *Polymer*, 2011, 52, 5-25.
- [33] A. Jorio. Raman spectroscopy in graphene-based systems: Prototypes for nanoscience
- [34] P. May, M. Lazzeri, P. Venezuela, F. Herziger, G. Callsen, J. S. Reparaz, A. Hoffmann, F. Mauri, J. Maultzsch. Signature of the two-dimensional dispersion in graphene probed by double-resonant Raman scattering. *Phys. Rev. B*, 2013, 87, 075402 (1-6).
- [35] S. Araby, I. Zaman, Q. Meng, N. Kawashima, A. Michelmoré, H.-Ch. Kuan, P. Majewski, J. Ma, L. Zhang. Melt compounding with graphene to develop functional, high performance elastomers. *Nanotechnology*, 2013, 24, 165601 (1-14).
- [36] M. Galimberti, M. Coombs, V. Cipelletti, P. Riccio, T. Ricco, S. Pandini, L. Conzatti. Enhancement of mechanical reinforcement due to hybrid filler networking promoted by anorganoclay in hydrocarbon-based nanocomposites. *Appl. Clay Sci.*, 2012, 65/66, 57-66.
- [37] A. Sadezky, H. Muckenhuber, H. Grothe, R. Niessner, U. Poschl. Raman micro-spectroscopy of soot and related carbonaceous materials: Spectral analysis and structural information. *Carbon*, 2005, 43, 1731-1742.
- [38] L. Bokobza, J. L. Bruneel, M. Couzi. Raman spectra of carbon-based materials (from Graphite to carbon black) and of some silicone composites. *C (J. Carbon Res.)*, 2015, 1, 77-94.
- [39] A. Merlen, J. G. Buijnsters, C. Pardanaud. A Guide to and review of the use of multiwavelength Raman spectroscopy for characterizing defective aromatic carbon solids: from graphene to amorphous carbons. *Coatings*, 2017, 7, 10, 153 (1-55).
- [40] A. Liu, L. Zhang, X. Yuan, X. Li, Y. Wu, X. Wang. Effect of ZrC formation on graphitization of carbon phase in polymer derived ZrC-C ceramics. *Mater.*, 2019, 12, 24, 4153 (1-13).